Supplementary Information

CryoEM of RUVBL1-RUVBL2-ZNHIT2, a complex that interacts with Pre-mRNA-processing-splicing factor 8

Marina Serna[1], Ana González-Corpas[1], Sofía Cabezudo[1], Andrés López-Perrote[1], Gianluca Degliesposti[2], Eduardo Zarzuela[1], J. Mark Skehel[2], Javier Muñoz[1] and Oscar Llorca[1*]

[1] Spanish National Cancer Research Centre (CNIO), Melchor Fernández Almagro 3, 28029 Madrid, Spain

[2] MRC Laboratory of Molecular Biology. Francis Crick Avenue. Cambridge Biomedical Campus, Cambridge, CB2 0QH. UK

[*] To whom correspondence should be addressed. Tel: +34 91 732 8000; Email: ollorca@cnio.es

Supplementary Figures and Tables

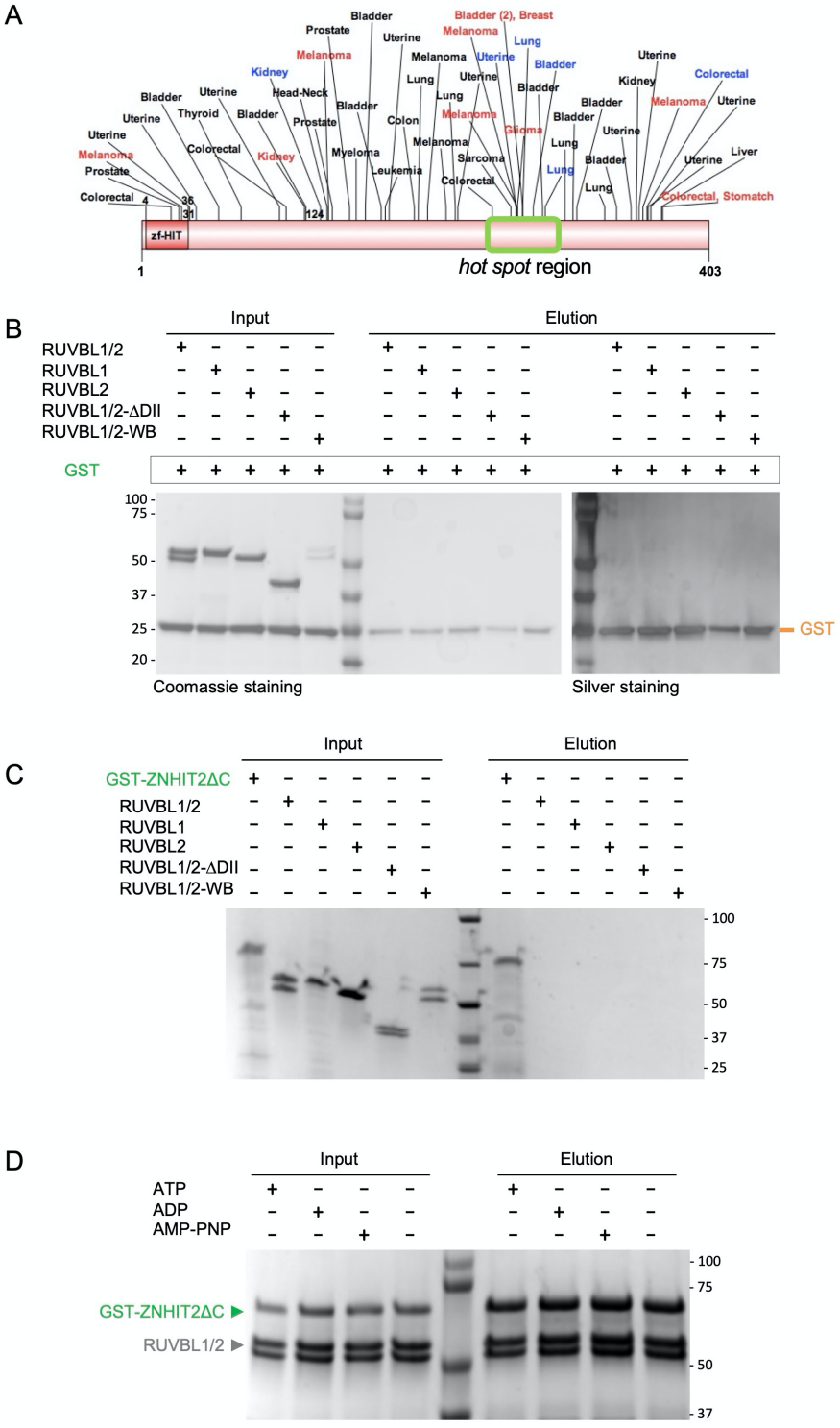

Supplementary Figure S1. ZNHIT2 and its interaction with RUVBL1-RUVBL2. (A) Cartoon of ZNHIT2 indicating mutations identified in several types of tumours according to cBioPortal (https://www.cbioportal.org/). A hotspot region is located between residues

280 and 300, and which are included in ZNHIT2ΔC and in the ZNHIT2-C construct used in this work. (B) SDS-PAGE showing inputs and the eluted material of the pull-down experiments shown in Figure 1D. These control experiments demonstrated that the GST tag in ZNHIT2ΔC does not introduce artifacts in the interactions detected for ZNHIT2ΔC. (C) SDS-PAGE showing inputs and eluted material of the of the pull-down experiments shown in Figure 1D, demonstrating that the bait proteins (RUVBL1, RUVBL2, RUVBL1-RUVBL2, RUVBL1/2-ΔDII, RUVBL1/2-WB) do not interact non-specifically with the GST binding resin. (D) Pull-down experiment controls of the GST-ZNHIT2ΔC protein with RUVBL1-RUVBL2 in the presence or absence of the nucleotides ATP, ADP or AMP-PNP. This experiment is shown in Figure 1E, but here we show the full experiment with input lanes that were omitted in the main figure to reduce the size of the figure.

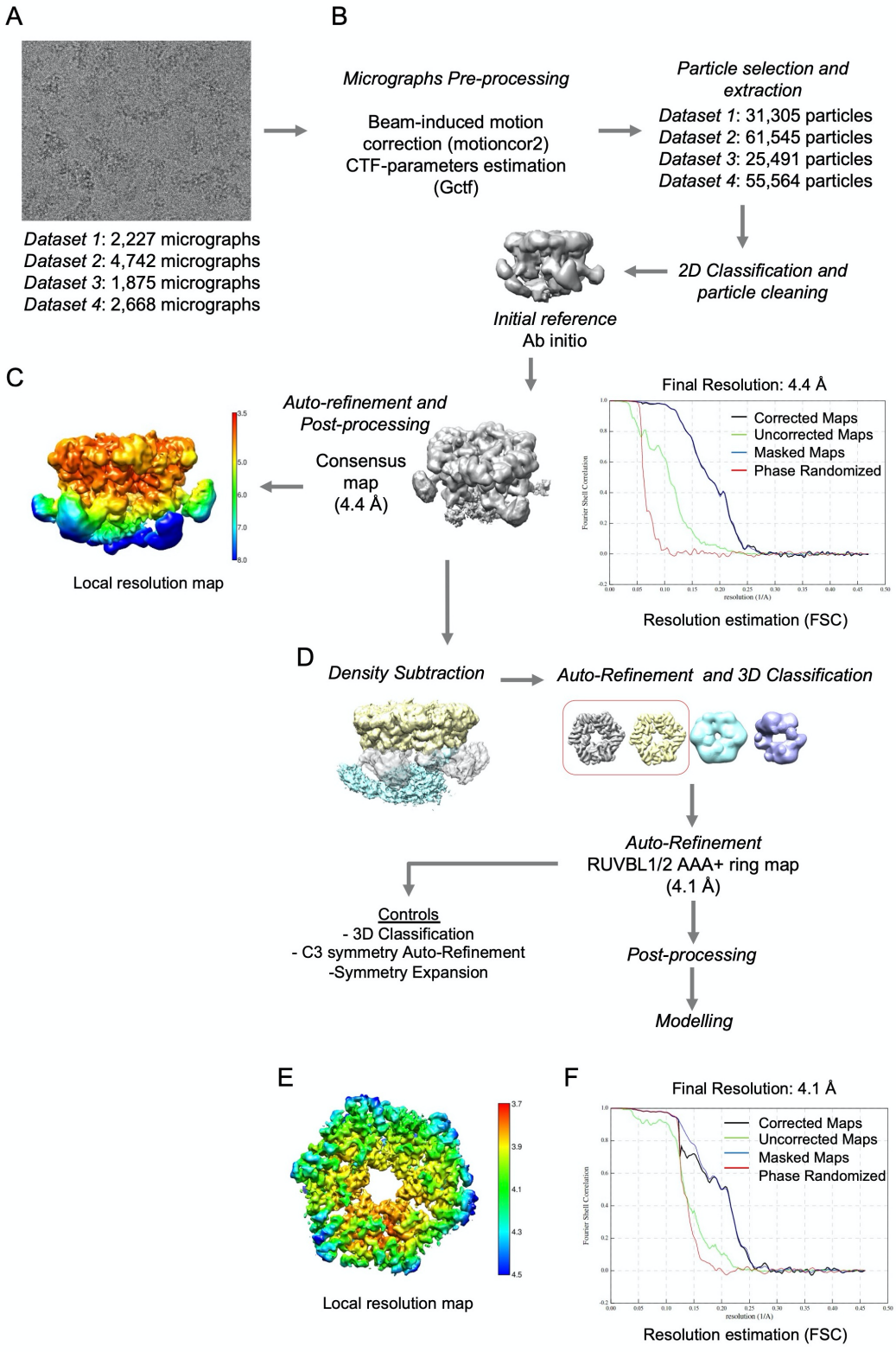

Supplementary Figure S2. CryoEM data collection and image processing of RUVBL1-RUVBL2-ZNHIT2ΔC. (A) Representative micrographs. (B) Pre-processing and initial image processing workflow. (C) Image processing workflow of the consensus map for

RUVBL1-RUVBL2-ZNHIT2ΔC. Right panel shows the resolution estimation using Fourier Shell Correlation (FSC) and a cut-off of 0.143 as provided by Relion. Left panel shows the local resolution estimation with the corresponding color scale. (D) Density subtraction protocol to analyse the RUVBL1-RUVBL2 hexameric ring independently. (E) Local resolution map for the RUVBL1-RUVBL2 ring extracted from the complex. Colour scale is shown at the right side of the map. (F) Estimation of the resolution using Fourier Shell Correlation (FSC) and a cut-off of 0.143 for the RUVBL1-RUVBL2 ring.

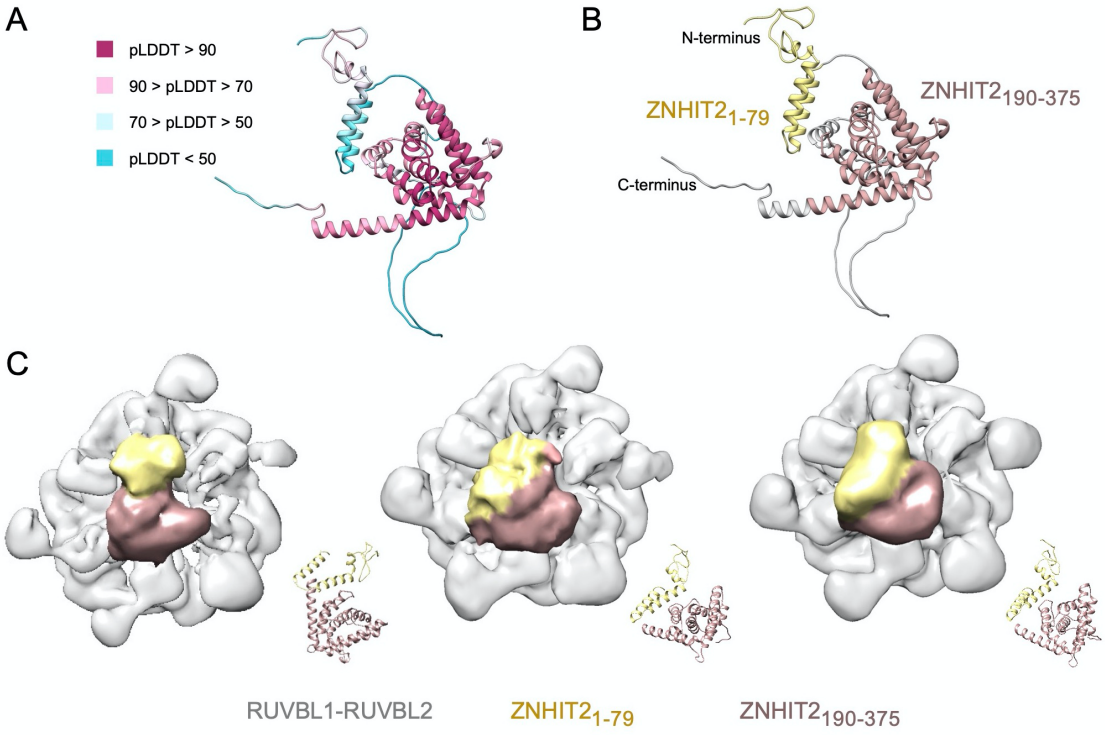

Supplementary Figure S3. Fitting of the predicted ZNHIT2 atomic model within the cryoEM density of ZNHIT2ΔC as part of the RUVBL1-RUVBL2-ZNHIT2ΔC complex. (A) Deepmind based atomic structure prediction of the human ZNHIT2 made by Alphafold (40). Ribbons in the structure are coloured according to the per-residue confidence metric pLDDT (colour code is included in the panel). (B) Representation of the regions present in the ZNHIT2ΔC sequence that were predicted with higher confidence. (C) The model shown in B was automatically adjusted within the RUVBL1-RUVBL2-ZNHIT2ΔC map by sequential fitting tools. The N-terminal region of ZNHIT2 (residues 1-79) is colored in yellow, and the C-terminal region (residues 190-375) is colored in light brown. Three selected cryoEM maps classified and reconstructed by cryoDRGN are shown, as examples of the flexible engagement of ZNHIT2ΔC to the RUVBL1-RUVBL2 hexameric ring. The unequivocal assignment of the globular domains of ZNHIT2ΔC to the N-terminal (yellow) and the C-terminal (light brown) regions is maintained along all the classes although its relative position with respect to the RUVBL1-RUVBL2 changes sensitively due to its inherent flexibility. The subclass shown at the left panel is the one selected for representation in Figure 2D-E. The low

resolution of the ZNHIT2ΔC density introduces some uncertainties to the experiment where the atomic model was fitted into the map. Because of this, we do not show the fitting of the atomic model of ZNHIT2ΔC within the cryoEM maps. Instead, we display the orientation of the atomic model after fitting within the ZNHIT2ΔC density in each of the subclasses, next to the corresponding map.

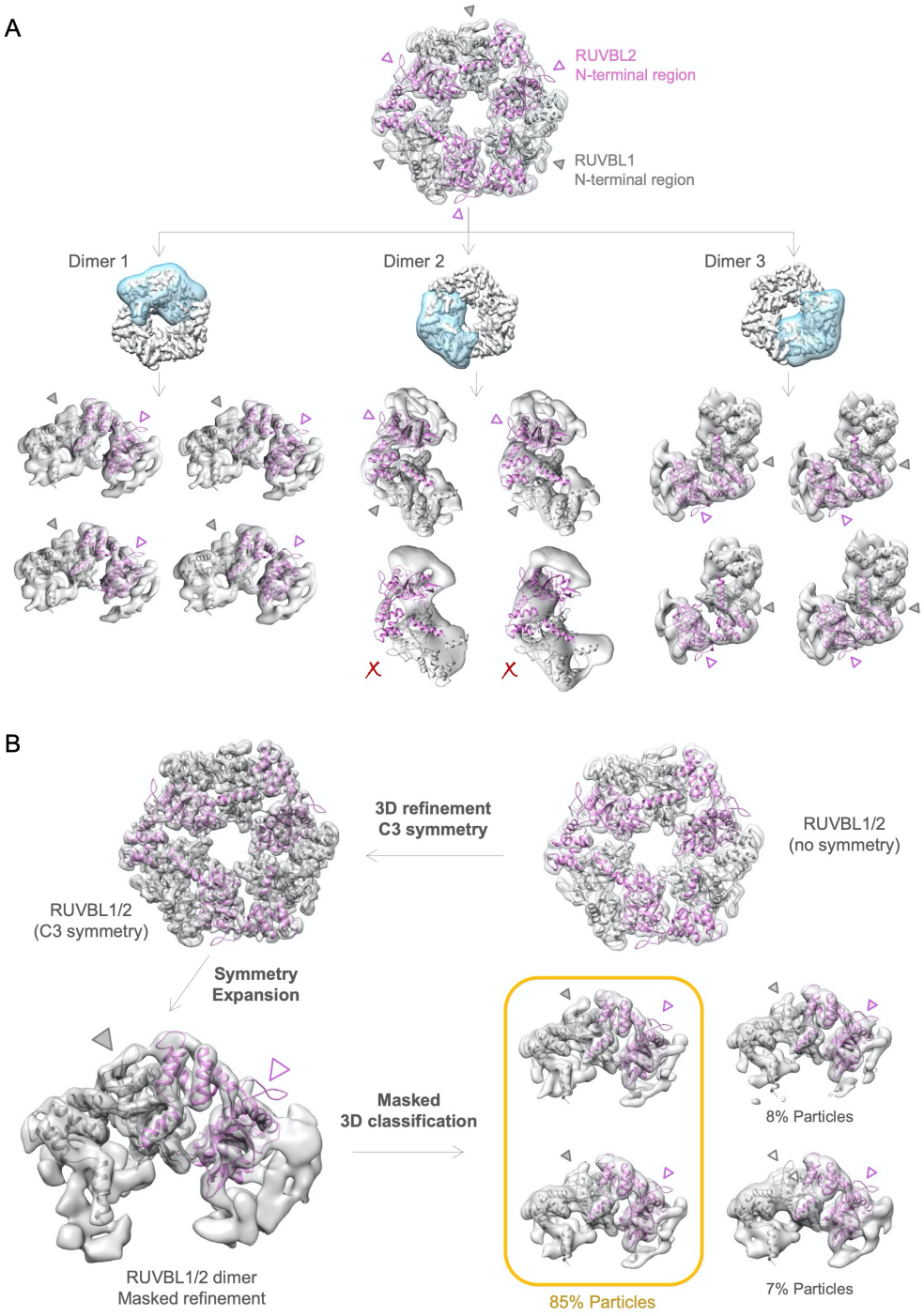

Supplementary Figure S4. Control experiments to verify that each RUVBL2 subunit in the RUVBL1-RUVBL2-ZNHIT2ΔC complex shows conformational changes in the His-Ser-His motif. (A) Focused 3D classification revealed the absence of density (empty pink arrowheads) assigned to the RUVBL2 N-terminal regions and the presence of the density belonging to the RUVBL1 N-terminal regions (full grey arrowheads) in the consensus map. Particles of the consensus 3D refinement and after applying a mask around each

RUVBL1-RUVBL2 dimer (semi-transparent blue density) were subjected to masked 3D classification. None of the classes obtained for each RUVBL1-RUVBL2 dimer showed density for the RUVBL2 N-terminal regions. Two of the classes obtained after classification of dimer #2 did not show enough density and resolution for most of the RUVBL1 and RUVBL2 subunits (red cross) and could not be interpreted. (B) The RUVBL1-RUVBL2 heterohexameric ring was refined imposing C3 symmetry and applying a symmetry expansion strategy as implemented in Relion. 3D reconstruction of a RUVBL1-RUVBL2 dimer obtained using the symmetry expanded particles was in agreement with previous observations, showing the absence of density that could accommodate the RUVBL2 N-terminal regions (empty pink arrowhead) and the presence of density corresponding to this region for RUVBL1 (full grey arrowhead). Subsequent 3D classification confirmed the complete (85 % particles) or partial (7 % particles) absence of the RUVBL2 N-terminal region in the density of the maps.

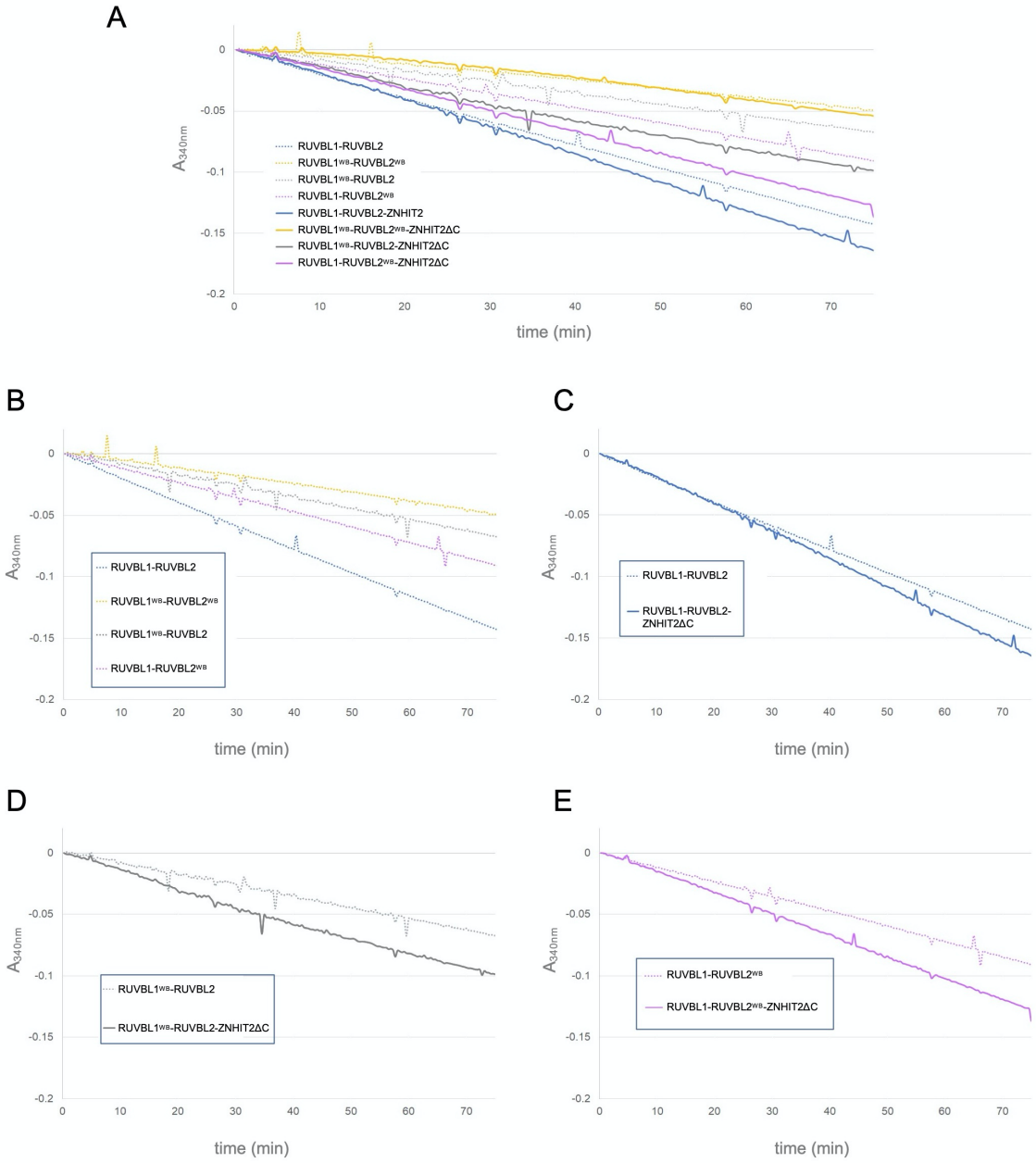

Supplementary Figure S5. ZNHIT2ΔC stimulates the ATPase activity of RUVBL1-RUVBL2. (A) Representative ATPase experiment showing a reduction in the absorbance of NADH at 340 nm with time as a result of the ATP consumption in the coupled enzymatic assay. The presence of ZNHIT2ΔC increased ATPase consumption rate for RUVBL1-RUVBL2 (blue line), RUVBL1$_{WB}$-RUVBL2, a RUVBL1 ATPase-dead mutant (grey line) and RUVBL1-RUVBL2$_{WB}$, a RUVBL2 ATPase-dead mutant (pink line). Significant ATPase activity was not measured for RUVBL1$_{WB}$-RUVBL2$_{WB}$, an ATPase dead mutant affected the Walker B domain in both subunits, regardless of the

presence or the absence of ZNHIT2ΔC (yellow line). Representative ATPase experiments for each of the samples when ZNHIT2ΔC was not added to the mix are shown: RUVBL1-RUVBL2 alone (dotted blue line), $RUVBL1_{WB}$-$RUVBL2_{WB}$, (dotted yellow line), $RUVBL1_{WB}$-RUVBL2 (dotted grey line) and RUVBL1-$RUVBL2_{WB}$ (dotted pink line). (B) ATPase experiments using each of the samples without ZNHIT2ΔC indicated a significant reduction in the ATPase activity for $RUVBL1_{WB}$-RUVBL2 and RUVBL1-$RUVBL2_{WB}$ with respect to wild type RUVBL1-RUVBL2, and no significant ATPase activity for $RUVBL1_{WB}$-$RUVBL2_{WB}$. (C) In the presence of ZNHIT2ΔC, we detected an increase in the ATP consumption rate in wildtype RUVBL1-RUVBL2 (blue line) with respect to the control experiment without adding ZNHIT2ΔC (dotted line). (D) ZNHIT2ΔC stimulates the ATPase activity of RUVBL2 in the $RUVBL1_{WB}$-RUVBL2 mutant (grey line) with respect to the control experiment without adding ZNHIT2ΔC (dotted line). (E) ZNHIT2ΔC increases the ATPase activity of RUVBL1 in RUVBL1-$RUVBL2_{WB}$ (pink line) with respect to the control experiment without ZNHIT2ΔC (dotted line), although the effect is less strong than for $RUVBL1_{WB}$-RUVBL2.

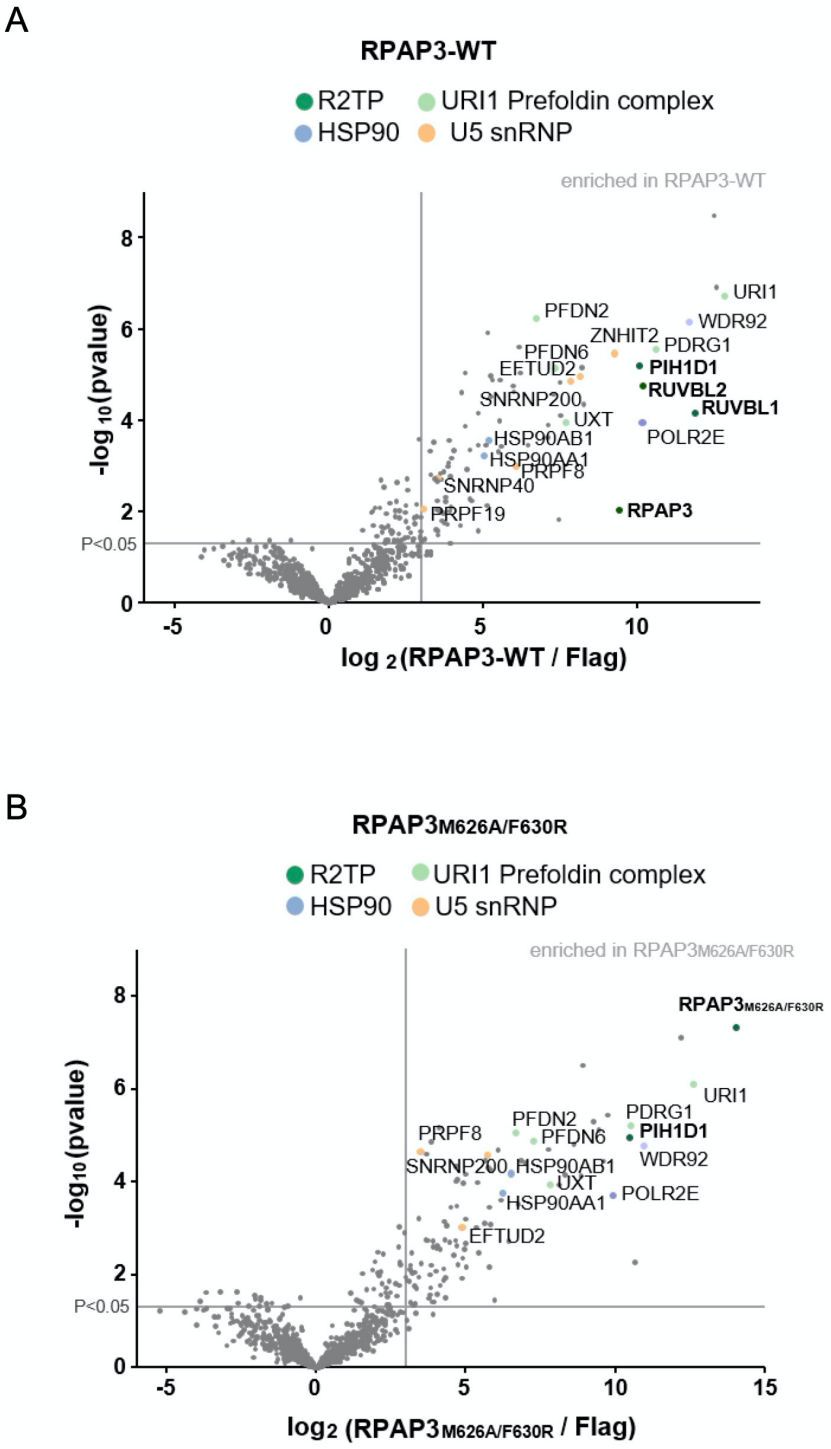

Supplementary Figure S6. The RPAP3 interactome in cells. (A) Volcano plot comparing interactors of RPAP3-WT versus IgG is shown. (B) Volcano plot comparing interactors of $RPAP3_{M626A/F630R}$ versus IgG is shown. In both cases, two-sample Student's T-Tests were performed and only proteins with a p-value<0.05 and a log2 ratio higher than 3 were considered as interactors.

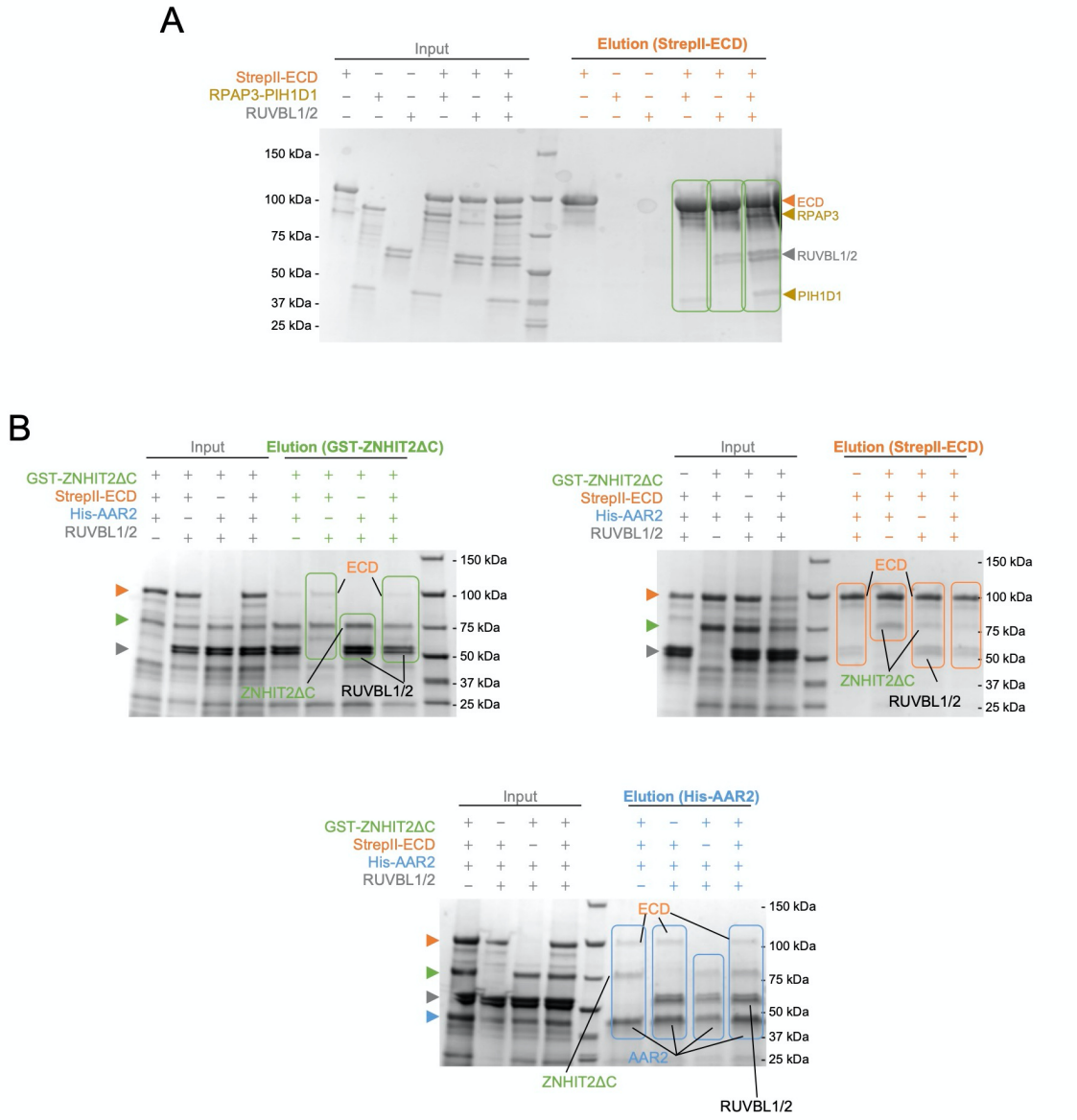

Supplementary Figure S7. Pull-down experiments using a combination of ZNHIT2ΔC, RUVBL1-RUVBL2, ECD, AAR2 and RPAP3-PIH1D1 proteins. (A) Pull-down experiment using the Strep II tag in ECD showed that the interaction of ECD with RUVBL1-RUVBL2 is stronger in the presence of RPAP3-PIH1D1, therefore allowing the assembly of the R2TP complex. Electrophoretic mobility of the purified proteins is shown with arrowheads. (B) Pull-down experiments using the GST tag in ZNHIT2ΔC (left panel, elution fractions labelled in green), the Strep II tag in ECD (middle panel, elution fractions labelled in orange) or the His tag in AAR2 (right panel, elution fractions labelled in blue). ECD and ZNHIT2ΔC associate also in the presence RUVBL1-

RUVBL2. These experiments also showed the formation of a complex between AAR2, ZNHIT2ΔC and ECD, and that this complex also occurs together with RUVBL1-RUVBL2. Electrophoretic mobility of the purified proteins is shown with arrowheads (ZNHIT2ΔC in green, ECD in orange, AAR2 in blue and RUVBL1-RUVBL2 in grey). In the pull-down experiments using GST-ZNHIT2ΔC and Strep II-ECD, the intensity of the bands for AAR2 in the experiments are weak and the bands runs in the same position than some contaminants present in the ZNHIT2ΔC preparation. Therefore, in these two experiments no conclusions could be made about AAR2. This was solved when His-AAR2 was pull-down since then the protein was enriched in the eluted material, and its coelution with ZNHIT2ΔC and ECD becomes evident (right panel).

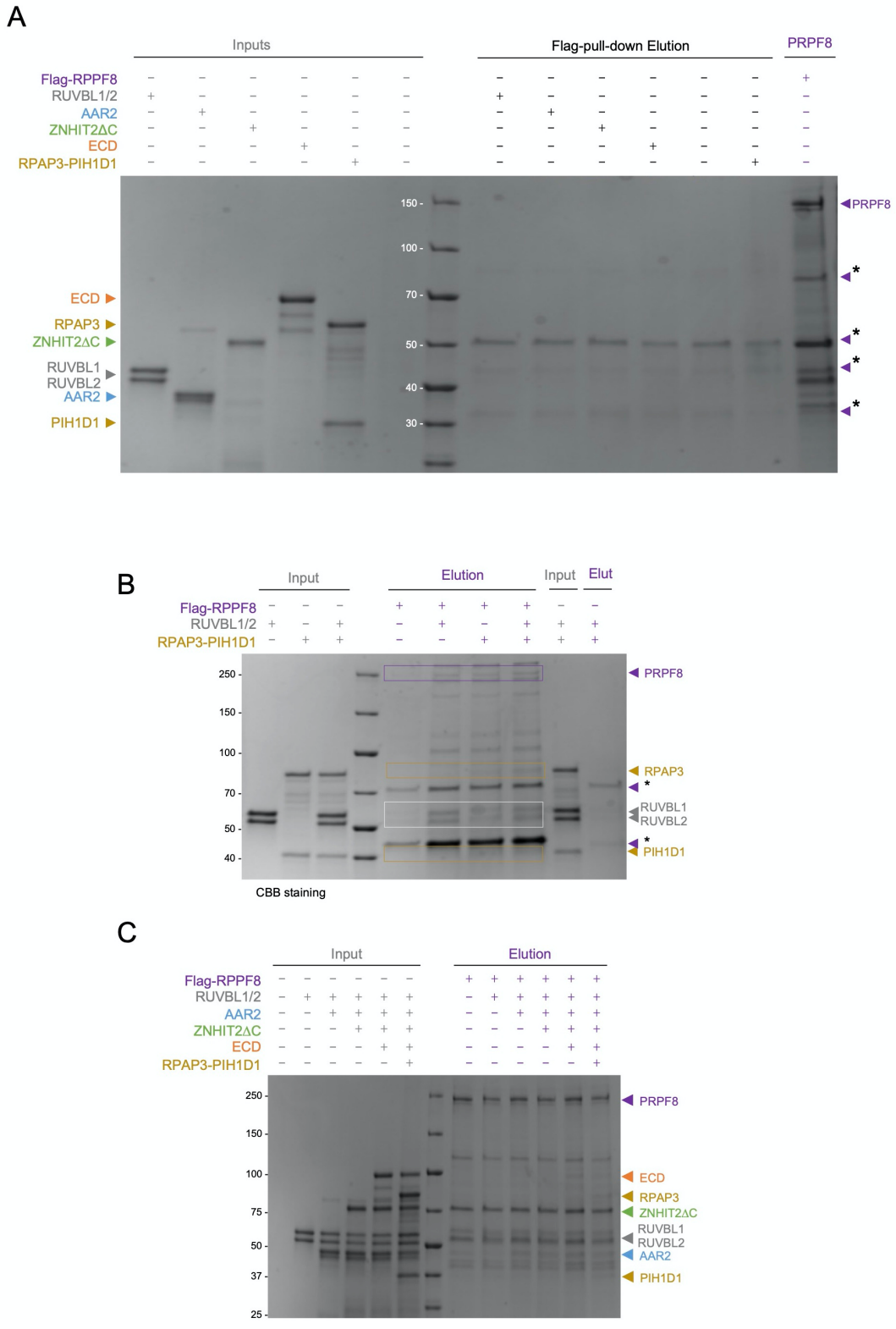

Supplementary Figure S8. Pull-down experiments using the Flag tag in PRPF8 suggests the existence of a multi-subunit complex containing PRPF8, AAR2, RUVBL1-RUVBL2,

RPAP3-PIH1D1, ZNHIT2ΔC and ECD. (A) Control for the experiments shown in Figure 6, showing that prey proteins used in the Flag-PRPF8 pull-down experiment (AAR2, RUVBL1, RUVBL2, RPAP3, PIH1D1, ZNHIT2ΔC and ECD) are not retained in the Flag affinity beads pre-loaded with a cellular extract without the heterologous overexpressed PRPF8. Asterisks indicate PRPF8 co-eluting contaminants. (B) SDS-PAGE of the Flag pull-down experiment shown in the upper panels of Figure 6B, where we observed that Flag-PRPF8 interacts with RPAP3-PIH1D1 in the presence or absence of RUVBL1-RUVBL2. (C) SDS-PAGE of the Flag pull-down experiment shown in Figure 6C, where we observed that RUVBL1-RUVBL2, RPAP3-PIH1D1, ZNHIT2ΔC, ECD and AAR2 (preys) co-eluted with Flag-PRPF8 (bait).

Table S1. Oligonucleotides used for cloning.

Construct	Name	Sequence 5'-3'
pGEX6P2-ZNHIT2**ΔC**	ZNHIT2 _FW	GGC GGA GAG AAT CTT TAT TTT CAG GGC ATG ACT TCA GCA AAT AAA GCA ATC GAA TTA CAA C
	ZNHIT2_REV	AGG TCC CTG GAA CAG CAC CTC CAG ACC ACG TAT CTT TTC TTG AGT TCT TCG
pGEX6P2-ZNHIT2-N	ZNHIT2_N _FW	TGA CCT CCA TGG CGG CCG TGG
	ZNHIT2_N_REV	CAG CAG CCG CCC GGC CTC
pGEX6P2-ZNHIT2-C	ZNHIT2_C _FW	TGA GCC CTC ACT GGG GAG
	ZNHIT2_C_REV	CCC AGT GAG GGC TCA GGC CAC CTC CTC G
pRSFduet1-His-AAR2	AAR2_FW	GAC TTT CTG AAC TAA AAA GGT TTG ATA TGG CAG TGA TGT TTA TGT CAG AAA C
	AAR2_REV	AAA CCT TTT TAG TTC AGA AAG TCT TTG TAA GAT TTC AAA GAT GAG T
pRSFduet1-His-AAR2-Strep II	AAR2_StrepII_FW	GTC CCT GGA ACA GCA CCT CCA G
	AAR2_StrepII_REV	GGC GGA GAG AAT CTT TAT TTT CAG GGC
pGEX6P2-RPAP3	RPAP3_FW	GAC TTT CTG AAC TAA AAA GGT TTG ATA TGG CAG TGA TGT TTA TGT CAG AAA C
	RPAP3_REV	AAA CCT TTT TAG TTC AGA AAG TCT TTG TAA GAT TTC AAA GAT GAG T
pRSFduet1-PIH1D1	PIH1D1_FW	GAC TTT CTG AAC TAA AAA GGT TTG ATA TGG CAG TGA TGT TTA TGT CAG AAA C

	PIH1D1_REV	AAA CCT TTT TAG TTC AGA AAG TCT TTG TAA GAT TTC AAA GAT GAG T
pACEmam_TEV_RPAP3_3C_3xFlag	RPAP3_cons_FW	GGC GGA GAG AAT CTT TAT TTT CAG GGC ATG ACT TCA GCA AAT AAA GCA ATC GAA TTA CAA C
	RPAP3_cons_REV	AGG TCC CTG GAA CAG CAC CTC CAG ACC ACG TAT CTT TTC TTG AGT TCT TCG
	Consensus_FW	CTG GAG GTG CTG TTC CAG GGA C
	Consensus_rev	GCC CTG AAA ATA AAG ATT CTC TCC GCC
pACEmam_TEV_RPAP3-M626A/F630R_3C_3xFlag	M626A/F630R_FW	GAC TTT CTG AAC TAA AAA GGT TTG ATA TGG CAG TGA TGT TTA TGT CAG AAA C
	M626A/F630R_REV	AAA CCT TTT TAG TTC AGA AAG TCT TTG TAA GAT TTC AAA GAT GAG T

Table S2. CryoEM data collection and image processing parameters

CryoEM data				
CryoEM data acquisition	Dataset 1	Dataset 2	Dataset 3	Dataset 4
Microscope	Thermo Scientific Titan Krios			
Camera	K2 (post-GIF)			
Magnification	130,000 x			
Stage Tilt	0º			
Voltage (kV)	300			
Micrographs	2,227	1,875	4,742	2,668
Exposure time (s)	8.0	8.0	9.0	8.0
Number of frames	40	40	40	36
Dose per frame ($e^-/Å^2$/frame)	1.00	1.00	1.035	1.15
Total Exposure ($e^-/Å^2$)	40.65	40	41.4	41.4
Defocus range (μm)	1.5-3.0	1.5-3.5	1.5-3.0	1.5-3.5
Original pixel size (Å/pixel)	1.047	1.065	1.09	1.047

CryoEM data processing	Consensus	RUVBL1-RUVBL2 AAA ring	ZNHIT2ΔC
Processing pixel size (Å/pixel)	1.409	1.065	1.409

Box size (pixels)	360	360	
Symmetry imposed	C1	C1	C1
Number particles	173,905	161,358	38,993
FSC threshold	0.143	0.143	0.143
Resolution (Å)	4.4	4.1	-
Resolution range (Å)	3.55-6.51	3.75-6.1	-
Map sharpening B-factor ($Å^2$)	-113	-115	-
Model building and refinement			
Model	RUVBL1-RUVBL2 AAA ring		
Initial model	Homology Model (PDB ID 6FO1)		
Model Composition			
Non-hydrogen atoms	14,168		
Protein residues	1,824		
Ligands	3 (ATP)		
R.m.s. deviations			
Bond length (Å)	0.0173		
Bond angles (º)	1.83		
Validation			
MolProbity score	2.07		
Clash score	18.54		
Poor rotamers (%)	0.91		
Ramachandran plot			
Favored (%)	96.36		
Outliers (%)	0.91		

Data deposition		
Database	Consensus	RUVBL1-RUVBL2 AAA ring
EMDB	EMDB-13233	EMDB-13233
PDB	-	PDB-7P6X

Table S3. Crosslinks between RUVBL1-RUVBL2 and ZNHIT2ΔC detected by cross-linked Mass Spectrometry (XL-MS).

Protein 1	Protein 2	Residue # (Protein 1)	Residue # (Protein 2)	Score
ZNHIT2	RUVBL1	325	268	80
ZNHIT2	RUVBL2	325	203	91
RUVBL2	RUVBL1	85	7	63
ZNHIT2	ZNHIT2	325	325	134
ZNHIT2	ZNHIT2	325	65	120
ZNHIT2	ZNHIT2	65	110	112
ZNHIT2	ZNHIT2	325	173	88
RUVBL1	RUVBL1	8	264	58
RUVBL1	RUVBL1	264	5	99
RUVBL1	RUVBL1	270	277	73
RUVBL2	RUVBL2	204	186	66
RUVBL2	RUVBL2	204	194	66

Table S4. Statistics on the RUVBL1-RUVBL2 ATPase assays.

Sample	N	Average	Standard Deviation	p
RUVBL1-RUVBL2	5	100	0	$p < 0.005$
RUVBL1-RUVBL2-ZNHIT2ΔC	5	112.985	5.211	
$RUVBL1_{WB}$-$RUVBL2_{WB}$	5	0.615	0.869	
$RUVBL1_{WB}$-$RUVBL2_{WB}$-ZNHIT2ΔC	5	1.235	1.746	
$RUVBL1_{WB}$-RUVBL2	5	11.9	3.210	
$RUVBL1_{WB}$-RUVBL2-ZNHIT2ΔC	5	36.9	10.281	
RUVBL1-$RUVBL2_{WB}$	5	31.955	17.275	
RUVBL1-$RUVBL2_{WB}$-ZNHIT2ΔC	5	52.93	31.211	